Geophysical Research Letters

RESEARCH LETTER
10.1029/2023GL106006

Strengthened ENSO Amplitude Contributed to Regime Shift in the Hadley Circulation

Juan Feng[1], Shuang Wang[1], and Jianping Li[2,3]

[1]State Key Laboratory of Remote Sensing Science, Faculty of Geographical Science, Beijing Normal University, Beijing, China, [2]Frontiers Science Center for Deep Ocean Multi-spheres and Earth System, Key Laboratory of Physical Oceanography, Academy of the Future Ocean, Ocean University of China, Qingdao, China, [3]Laoshan Laboratory, Qingdao, China

Key Points:

- The principal mode of boreal winter Hadley circulation (HC) during recent 4 decades shows a regime shift and is dominated by an equatorially symmetrical pattern
- The strengthened El Niño–Southern Oscillation (ENSO) explains the spatiotemporal variation and regime shift of the HC variability
- Model simulations indicate that their ability to reproduce the ENSO variability is a key factor in determining HC variability

Supporting Information:

Supporting Information may be found in the online version of this article.

Correspondence to:

J. Feng and S. Wang,
fengjuan@bnu.edu.cn;
wangshuang6@mail.bnu.edu.cn

Citation:

Feng, J., Wang, S., & Li, J. (2024). Strengthened ENSO amplitude contributed to regime shift in the Hadley circulation. *Geophysical Research Letters*, *51*, e2023GL106006. https://doi.org/10.1029/2023GL106006

Received 23 AUG 2023
Accepted 27 DEC 2023

Abstract Understanding the variability in the Hadley circulation (HC) changes is crucial for understanding ocean-atmosphere interactions. In this study, the variability in the boreal winter HC in the last 4 decades is explored using multiple reanalyzes and model simulations. The results show that regime shift occurred in the leading mode of HC variability. The primary mode of the recent HC is dominated by an equatorially symmetrical pattern, which was considered the second mode in previous studies. The regime shift in HC variability is mainly due to the El Niño–Southern Oscillation (ENSO), which explains both the spatiotemporal variation and formation of HC variability. Moreover, the abilities of the models to reproduce HC variability is subject to their ability to simulate ENSO variability, suggesting that the ENSO has become a more important modulator of the HC variability in recent decades, and additional research is warranted to evaluate future climate changes and potential effects on the HC.

Plain Language Summary The Hadley circulation (HC) has significant regulatory impacts on tropical and extratropical interactions. As a thermal-dynamical circulation, the variability in the HC exhibits a substantial correlation with the underlying thermal conditions. However, strong interdecadal variations have been observed in the tropical sea surface temperature (SST) around 1976/1977, particularly in the SST related to the El Niño–Southern Oscillation (ENSO). The HC variability after 1977 is still unknown. We investigate the spatial-temporal variation in the boreal winter HC during the period of 1980–2020. The results show that the primary dominant mode (EOF1) of the HC presents an equatorially symmetrical structure with ascension around the equator. This pattern corresponds to the second dominant mode in preceding studies. The different result indicates that a regime shift in HC variability has occurred. We find that the formation of EOF1 is due to the enhanced variation in ENSO, which explains the spatial-temporal variations in EOF1. This result is further confirmed in model simulations, highlighting a more important role of the ENSO on the HC in recent decades. These results deepen our understanding of HC variability and emphasize the important climatic effects of the ENSO, which is of great interest because more severe ENSO events are projected for the future.

1. Introduction

The El Niño–Southern Oscillation (ENSO) phenomenon is the dominant mode of tropical climate variability, exerting a pivotal influence on global weather and climate anomalies (e.g., Klein et al., 1999; Trenberth et al., 1998; Wallace et al., 1998). Previous studies show that El Niño has substantial impacts on tropical and extratropical oceans and atmospheric circulations via atmospheric bridges (Alexander et al., 2002; Lau, 1997), oceanic teleconnections (Clarke & Van Gorder, 1994), and air-sea coupled bridges (Y. Li et al., 2019). However, significant interdecadal variations are reported in the relationships between the ENSO and its related climatic variabilities. For example, interdecadal shifts are observed in the associations between the ENSO and North Atlantic Oscillation (S. Hu et al., 2023; Zhang et al., 2021), precipitation over the USA (Gutzler et al., 2002; Higgins et al., 2000), sea surface temperature (SST) over the tropical Indian Ocean (Terray & Dominiak, 2005; Wang & An, 2001), and the Indian summer monsoon (Krishnamurthy & Goswami, 2000; K. K. Kumar et al., 1999). These interdecadal variations in the ENSO-related connections are partly because the ENSO itself exhibited an interdecadal change (McPhaden et al., 2011; Zhang et al., 2019). Extensive evidence has indicated that the meridional extent (Zhang et al., 2013), temporal evolution (Z. Hu et al., 2013; A. Kumar & Hu, 2014), period (Fedorov & Philander, 2001), intensity (Gong et al., 2020; Grothe et al., 2020), and propagation direction (Lu et al., 2022) of the ENSO have changed around 1976/1977. Consequently, the interdecadal variation in the ENSO may trigger

corresponding changes in climatic variabilities and regional climate anomalies, particularly in systems whose variability is closely associated with the ENSO.

The Hadley circulation (HC) is a highly important, large-scale atmospheric circulation at low latitudes, which transports more heat, angular momentum, and mass from the tropics to the extratropics than do transient and steady vortices and contributes to tropical and extratropical climate anomalies (e.g., Chang, 1995; Feng & Li, 2013; Held, 2001). As a thermal-dynamical circulation, the HC intensity (HCI) is tightly attached to underlying thermal conditions. An enhanced HC is expected to be observed during El Niño winters, whereas a suppressed HC is seen in La Niña winters (e.g., Nguyen et al., 2013; Oort & Yienger, 1996). The ENSO impacts the HCI by inducing anomalous meridional circulation, which in turn affects the spatial-temporal variability of the HC. The interannual variability in the seasonal HC is predominantly controlled by two leading modes (e.g., Feng et al., 2013; Guo et al., 2016; Ma & Li, 2008; Sun & Zhou, 2014); the first mode is characterized by a single cross-equatorial cell with opposite vertical motions on each side (equatorially asymmetrical mode, AM; Figures S2a and S2b in Supporting Information S1), and the second mode features a pair of cells with a combined ascending branch around the equator (equatorially symmetrical mode, SM; Figures S2c and S2d in Supporting Information S1). Of note is that the AM and SM are consistently observed in both the annual cycle and interannual variability (e.g., in period 1948–1979 and 1948–2010 as reported) of the HC, inferring that the AM and SM are not sensitive to the sample length. Meanwhile, considering that the meridional distribution of HC is subjected to the underlying meridional gradient of tropical SST (Feng et al., 2023; E. Schneider & Lindzen, 1977), an equatorially asymmetrical/symmetrical SST distribution would associate with equatorially asymmetrical/symmetrical HC anomalies. It is established that the AM variation is attached to SST over tropical Indian Ocean (Feng et al., 2013; Ma & Li, 2008), whose formation is due to the inhomogeneous warming trend over this region (J. Li & Feng, 2015). And the SM variation is closely linked to the ENSO because SST anomalies associated with the ENSO are equatorially symmetrical (Guo & Tan, 2018; Sun et al., 2019). In later research, the effect of the ENSO on HC modes is shown to be dependent on the ENSO phase; a strengthened SM is observed along with El Niño but only during its developing phase, whereas an intensified AM is seen during its decaying phases (Feng et al., 2023). This can be mainly attributed to the occurrence of anomalous equatorially asymmetrical SST over the eastern Pacific and Indian Oceans in the El Niño decaying phase (Feng et al., 2023; McGregor et al., 2013). These findings highlight the importance of the ENSO in modulating HC variability; however, the connections between the ENSO and HC vary along with the ENSO phases.

In addition to the developing and decaying phases, the mature phase is the vital time period of ENSO events and is accompanied by the strongest SST anomalies (Chen & Jin, 2020; Peng et al., 2020). Although preceding studies have examined ENSO impacts on HC during its mature phase mainly focused on the HC's intensity (e.g., J. Li & Feng, 2015; Oort & Yienger, 1996), potential influences of interdecadal variation in the ENSO on the HC's variability have not been reported. Substantial interdecadal variations are detected in the intensity, period, and meridional scale of the ENSO around 1976/1977, and such interdecadal changes would inevitably change the corresponding SST distributions (Capotondi & Sardeshmukh, 2017; Deser et al., 2012), thus affecting the HC variability. However, the characteristics of the HC variability following the interdecadal variation in ENSO are still unknown, as is the extent to which the ENSO interdecadal variation affects the HC variability and whether the current climate models can reproduce these associated variations. Here, we address these questions and investigate the characteristics of boreal winter (December–February) HC variability after the interdecadal variation in the ENSO using multiple reanalyzes and ensembles of model outputs.

2. Data and Methods

The monthly average atmospheric variables used are from JRA55 (Kobayashi et al., 2015), MERRA2 (Gelaro et al., 2017), ERAI (Dee et al., 2011), ERA5 (Hersbach et al., 2020), CFSR (Saha et al., 2010), and NOAA–20CR (Compo et al., 2011), and the SST data set is from HadISST (Table S1 in Supporting Information S1, Rayner et al., 2003). In addition, the NCEP1 (Kalnay et al., 1996) and NOAA–20CR are used to examine the HC variability before 1980. The Niño 3.4 index (an area-averaged SST over 5°S–5°N, 120°–170°W) is employed to depict the variability in the ENSO. Seventeen Atmospheric Model Intercomparison Project (AMIP) models (Table S2 in Supporting Information S1) and 20 Coupled Model Intercomparison Project (CMIP) models (Table S3 in Supporting Information S1) from CMIP6 are employed due to the availabilities. Only one member (r1i1p1) is selected in each model. The AMIP is directed by the real-time SST as the boundary forcing, facilitating a feasible

simulation to investigate the impacts of SST on the circulation. To obtain the ensemble average of the models, the individual models are interpolated to the same horizontal and vertical resolutions.

The HC can be characterized by mass stream–function (MSF, Oort & Yienger, 1996). It represents the vertical integration of the zonally averaged meridional winds, providing a quantitative depiction of the global meridional circulation,

$$\psi(\varphi, p) = \frac{2\pi a \cos\varphi}{g} \int_0^p \left[\overline{v}(\varphi, p)\right] dp$$

where v is meridional wind, a is the radius of the Earth, p is pressure, φ is latitude, and g is Earth's gravity. The [ ] and $\overline{\ }$ operators represent zonal and temporal averaging, respectively. The empirical orthogonal function is employed to detect the primary mode (EOF1) and the corresponding principal component (PC1) of the boreal winter HC. Correlation and partial correlation analyses were employed to detect the relationship between the tropical SST and HC. The partial correlation is a measure of the linear dependence between two variables where the influence from possible controlling variables is removed (Freund & Wilson, 2003). The detailed method is as follows:

$$r_{ij,k} = \frac{r_{ij} - r_{ik} r_{jk}}{\sqrt{\left(1 - r_{ik}^2\right)\left(1 - r_{jk}^2\right)}}$$

Where r_{ij} represents the correlation coefficient between variables i and j, r_{ik} represents the correlation coefficient between variables i and k, and r_{jk} represents the correlation coefficient between variables j and k. In this study, i represents HC PC1, j represents SST, and k represents the Niño 3.4 index. The Niño 3.4 index is selected as the controlling variable in partial correlation to show the contributions of the ENSO to the relationships between HC PC1 and SST. The statistical significance of the correlation values is evaluated using Student's t test.

3. Results

Climatological distributions of the boreal winter HC and its EOF1 are displayed in Figure 1. These six reanalyzes indicate a consistent spatial characteristic in the climatological distribution, with a spatial correlation coefficient above 0.99 across different data sets (Figure S2a in Supporting Information S1). The northern cell exhibits dominance in the climatological boreal winter HC, with a combined ascending branch at approximately 12°S, and the two descending branches manifest near latitudes of approximately 30°N and 35°S within each hemisphere. That is, the climatological winter HC exhibits an equatorially asymmetrical pattern, indicating a transfer of mass from the northern to southern hemispheres through the lower troposphere (Kang et al., 2008; T. Schneider et al., 2014). However, EOF1 of the HC exhibits a quasi-symmetrical distribution around the equator, explaining ∼39% of the variance, showing combined ascending around the equator and two descending branches at approximately 25°S and 15°N in each hemisphere. A similar result is observed in the detrended data sets across different reanalyzes. Note that this pattern is consistently observed across the six reanalyzes even the length of the data sets is different (Table S1 in Supporting Information S1), with the spatial correlation exceeding 0.89 across different data sets (Figure S2b in Supporting Information S1), thereby underlying the robustness of this mode. Although the strength of the northern cell is greater than that of the southern cell (paralleling the stronger climatological northern cell), the spatial structure and extent of the two cells are equivalent, resembling the distribution of SM (Ma & Li, 2008; Figures S1c and S1d in Supporting Information S1). Of note is that the first leading mode of the variability of boreal winter HC before 1980 is an AM, while the second leading mode exhibits a SM (Figure S1 in Supporting Information S1). The above result suggests that SM replaces AM in the last 40 years and turns into the primary source of variability of the HC in boreal winter, indicating that regime shift has occurred in the boreal winter HC variability. In addition, the opposing distributions of EOF1 to the north and south of the equator are different from its climatological distribution, implying a narrowing and northwards shift of the ascending branch (Byrne et al., 2018; Hari et al., 2020). Consequently, this northwards ascension would induce a shift in convection and precipitation during this season.

Correspondingly, the temporal variation in this mode is examined (Figure 1g). The PC1 shows strong interannual variation without obvious linear trends. The three strongest values in PC1 occur in the winters of 1982, 1997, and 2015, which all coincide with well-defined El Niño events. This suggests that the EOF1 variation may be

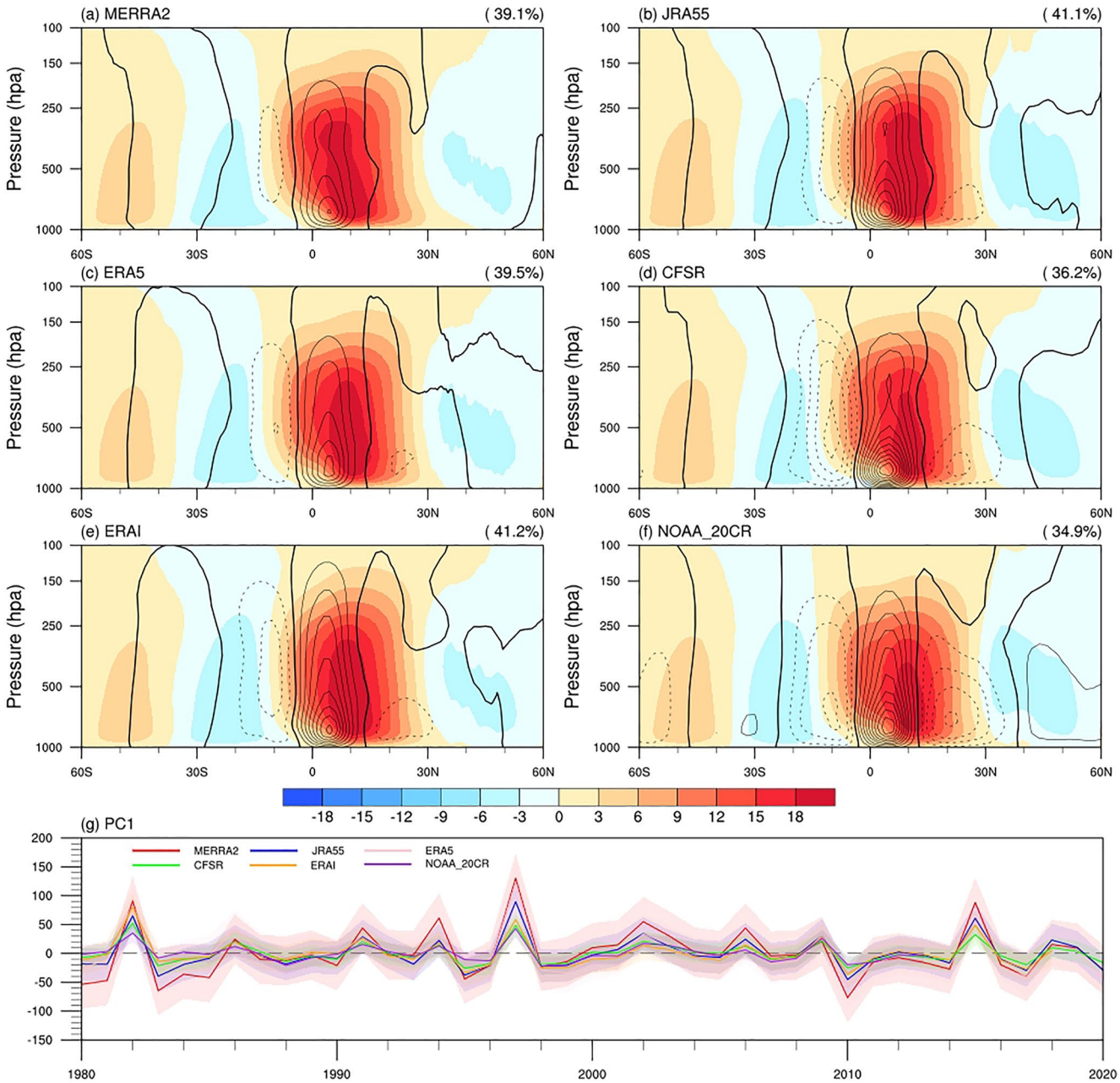

Figure 1. The climatological mean of the boreal winter mass stream–function (shading) and its principal mode (EOF1, contour) determined from (a) MERRA2, (b) JRA55, (c) ERA5, (d) CFSR, (e) ERAI, and (f) NOAA–20CR. The contour interval is 0.03×10^{10} kg/s. Solid (dotted) contours are positive (negative) and the zero contour is thickened. The number is the corresponding explained variance. (g) Time series for EOF1 of the boreal winter Hadley circulation (solid line). The shading for each data set is referenced to its one standard deviation.

connected to the ENSO. Moreover, it is seen both the EOF1 and PC1 based on the six data sets are highly consistently with each other (Figure S1 in Supporting Information S1), thus only the result based on the JRA55 is shown. The relationship between EOF1 and the underlying SST is further explored by examining their linear correlations (Figure 2a). In the tropical eastern and central Pacific and tropical Indian Ocean, significant positive correlations are observed, contrasting with negative correlations observed in the western Pacific, presenting a classical ENSO pattern. This finding is additionally supported by the high correlation coefficient between PC1 and the Niño 3.4 index, with a coefficient exceeding 0.77 across different data sets (Figure 3b). Note that the substantial relationship between PC1 and the Niño 3.4 index is robust for both the positive and negative values of the Niño 3.4 index, suggesting that no asymmetry exists in this relationship. We further examine the relationship between

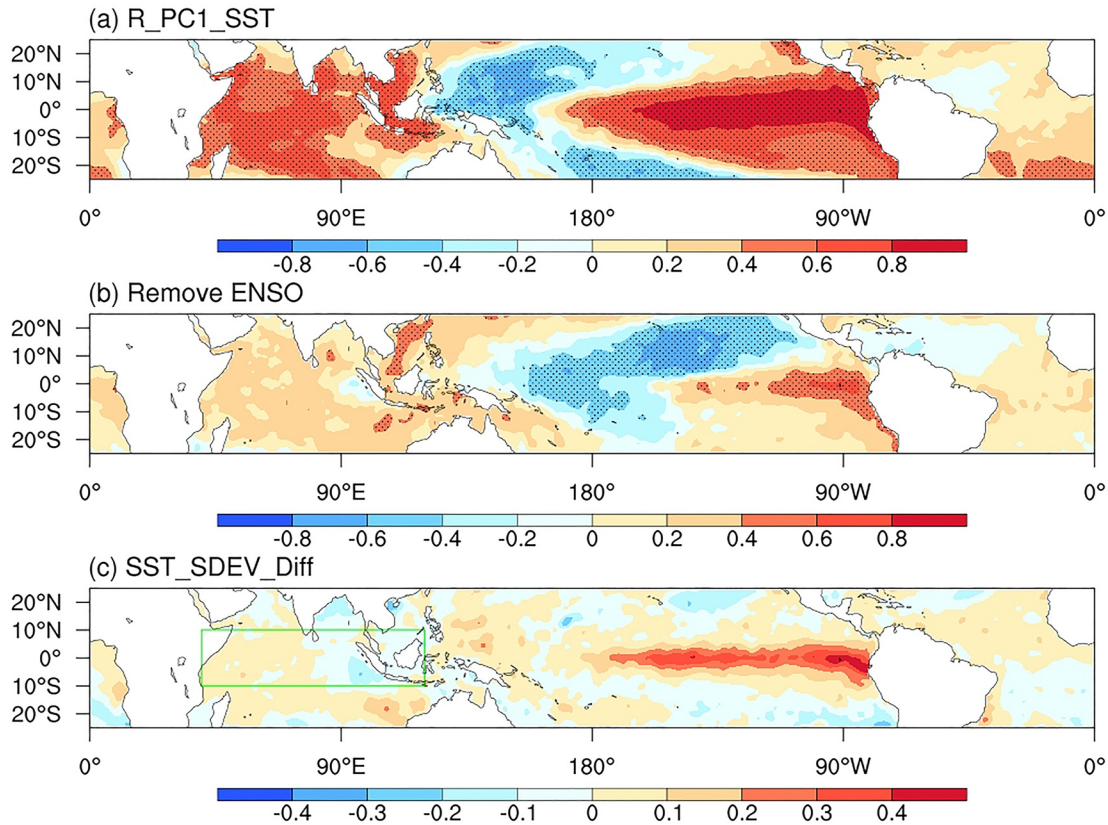

Figure 2. (a) Correlation between PC1 and boreal winter sea surface temperature (SST). (b) Same as (a), but without the El Niño–Southern Oscillation effect. Dark spots indicate significant values at the 0.05 level. (c) The difference in the standard deviation of SST between the periods of 1980–2020 and 1948–1979. The green rectangle represents the selected tropical Indian Ocean region (40°–120°E, 10°S–10°N).

PC1 and other extratropical climate variabilities (i.e., the North Atlantic Oscillation, the Atlantic Multidecadal Oscillation, and the Pacific Decadal Oscillation), showing insignificant relationships. That is the role of the extratropical signals on the HC EOF1 is not as important as that of the ENSO. Moreover, the significant linkage between tropical SST and EOF1 almost disappears when the effects of the ENSO are removed (Figure 2b), further revealing that the significant correlations between tropical SSTs and EOF1 are mainly due to the ENSO. The significant linkage between the ENSO and EOF1 not only accounts for the temporal evolution of PC1 but also explains the spatial distribution of EOF1. In the lower troposphere, the spatial distribution of the meridional circulation is mainly subjected to the meridional structure of the SST (e.g., Feng & Li, 2013; Numaguti, 1994; E. Schneider & Lindzen, 1977). The SST anomalies related to El Niño and La Niña events during their mature phases are equatorially symmetrical (Feng et al., 2019; Zhang et al., 2013), favoring equatorially symmetrical meridional circulation anomalies and contributing to EOF1 formation. That is, the spatial-temporal variation in the ENSO exerts a significant influence on the HC variability.

Moreover, the simulated climatological HC as well as its primary mode from 17 AMIP models are checked to verify the contribution of the underlying SST to the formation of HC variability. The simulated climatological HC agrees with the reanalyzes, which is evident through significant correlations as well as standard deviation ratios (Figure S3 in Supporting Information S1). Consequently, the ensemble mean is employed to investigate the variability of the HC, as shown in Figure 3. The ensemble EOF1 agrees with the reanalyzes and exhibits an equatorially symmetrical structure, showing significant spatial correlations with the reanalyzes with coefficients exceeding 0.90. Note that the simulated HC EOF1 bears an even greater explained variance (64%) than that of the reanalyzes, highlighting the impacts of underlying SSTs on HC variability. This greater explained variance value is because only ocean-driven atmospheric circulation is considered in the AMIP; however, strong air-sea interactions are involved during an ENSO event, and the HC also shows strong feedbacks on the ENSO (S. Hu & Fedorov, 2018; Peng et al., 2019, 2020). Nevertheless, the high similarity between the reanalyzes and AMIP simulation highlights the contribution of the SST on the formation of EOF1 of the HC.

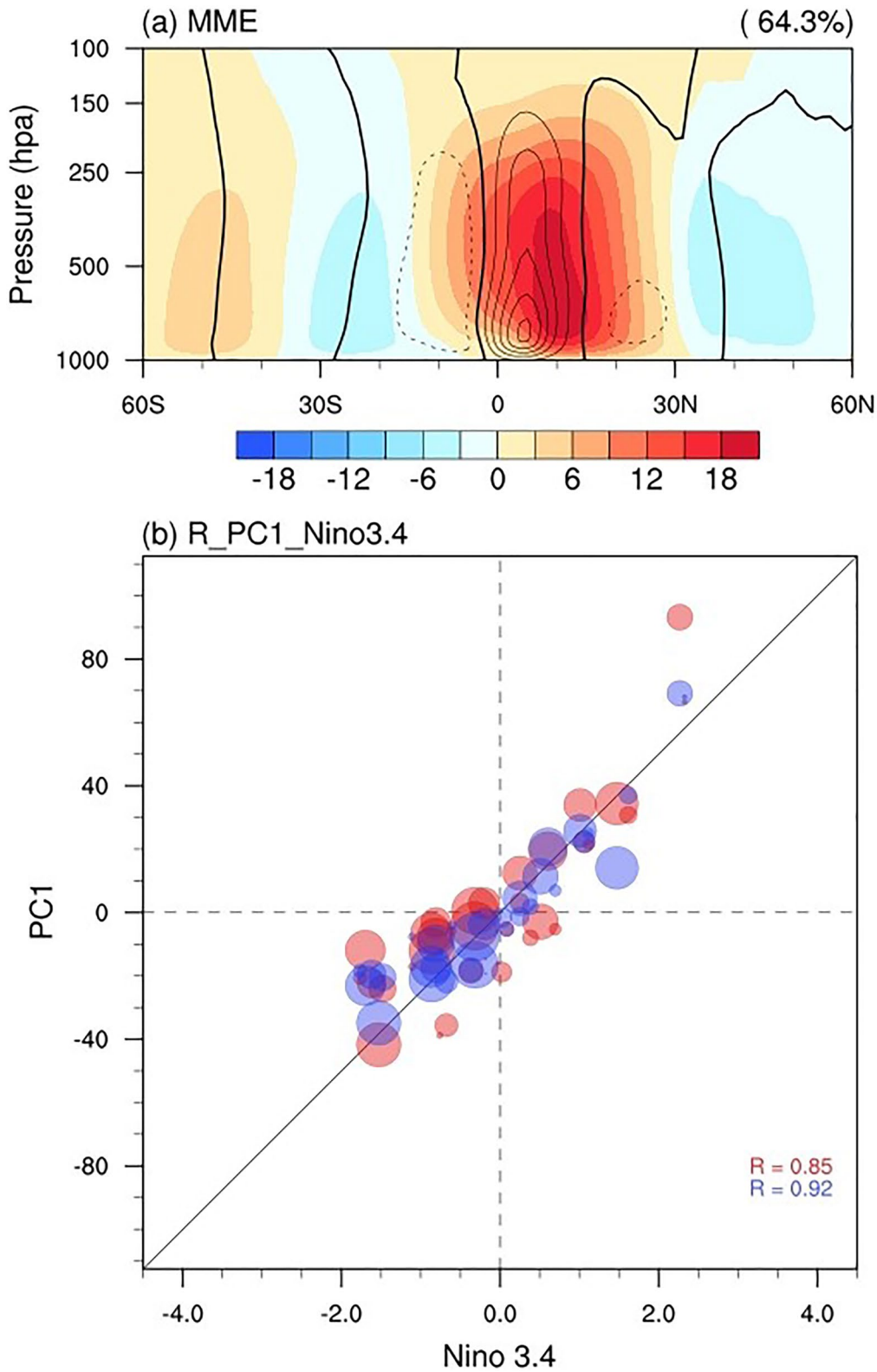

Figure 3. (a) Same as Figure 1a, but for the ensemble average from 17 Atmospheric Model Intercomparison Project (AMIP) models. (b) Scatter plot of the Niño 3.4 index versus the Hadley circulation PC1 (red) and the AMIP ensemble mean (blue). *R* indicates the correlation coefficient. The diameter of the bubble represents the sequence of years in the PC1, the larger bubbles indicate the later of the year.

The possible contribution of the ENSO to the formation of EOF1 is explored above. However, it is still unknown why the SM could replace the AM and become the first leading mode of HC variability. To answer this question, we analyze the interdecadal variations in tropical SST variability by exploring the difference in its standard deviations between 1980–2020 and 1948–1979 (Figure 2c). Compared with that in the tropical Indian Ocean, the SST variability within the tropical central and eastern Pacific is significantly enhanced (Y. Li et al., 2019, 2021). As reported, the AM variation is mainly attached to the SSTs within the tropical Indian Ocean. We further analyze the standard deviation in the areal mean SST over the Indian Ocean (40°–120°E, 10°S–10°N; the green rectangle in Figure 2c) as well as that in the Niño 3.4 index. The standard deviation in the Niño 3.4 index largely increases in the period after 1979 (1.09°C vs. 0.86°C), while there is little change in the tropical Indian Ocean SST (0.26°C vs. 0.25°C). That is, the variability in the ENSO has been largely enhanced in the last 40 years, replacing the SST in the tropical Indian Ocean as the dominant factor in impacting the variability of the boreal winter HC. This finding shows that increased ENSO variability may be a possible cause for the regime replacement of the HC during the last 40 years.

We further use the CMIP6 model output to investigate the effect of the ENSO on HC variability. We divide all CMIP6 models into two groups according to their ability to reproduce HC EOF1: that is, the well-simulated group (Type I), with spatial correlation coefficients exceeding 0.5 between the simulated and observed EOF1, and the remaining models fall into the Type II group (Figure S3d in Supporting Information S1). The result is not sensitive to the chosen threshold value, similar result is seen for a threshold value 0.60. The 0.50 is chosen as the threshold is for a greater sample size. The classification of the two groups of models is detailed in Table S3 in Supporting Information S1. Subsequently, the ensemble mean of the two groups of models is determined. The results of HC EOF1 simulated by the models are shown in Figure 4. We see that the Type I models can well reproduce the spatial characteristics of HC EOF1, with a 0.83 spatial correlation coefficient with the observation. In contrast, EOF1 of the Type II models shows an asymmetrical structure (showing a 0.03 spatial correlation coefficient with the observation), exhibiting a large bias with the reanalyzes. The better simulation ability of HC EOF1 in Type I models is mainly due to their better performance in reproducing the ENSO variability. The standard deviation of the simulated Niño 3.4 index is close to that of the observations (1.17°C vs. 1.09°C). In this way, the Type I models well reproduce the association between PC1 and tropical SST (figure not shown), as well as the relationship with the Niño 3.4 index. However, the Type II models underestimate the ENSO variability, and the relationship between PC1 and the tropical SST are not captured (figure not shown), either the connection with the Niño 3.4 index. This result indicates that the simulation performance of the ENSO variability determines a model's ability to reproduce the variability in the HC and further indicates that the variability in the ENSO is an important factor affecting the spatiotemporal variation in HC EOF1.

4. Conclusion and Discussion

We investigate the variability in boreal winter HC during the last 40 years in this study. The primary mode of the HC exhibits an equatorially symmetrical pattern, which was considered the second leading mode in previous studies (e.g., Guo & Tan, 2018; Ma & Li, 2008). The replacement of the sequence in the leading modes suggests that a regime shift has occurred in the HC variability. This result is consistent across six different reanalyzes, implying the robustness of the regime replacement findings in HC variability. The regime shift in HC variability is accurately captured in the AMIP models, indicating that the variation in the HC is mainly connected with underlying thermal conditions.

The ENSO explains the spatial and temporal variation in the HC EOF1. In terms of the spatial distribution, ENSO-related SSTs exhibit an equatorially symmetrical pattern, which is associated with the equatorially symmetrical circulation (Bordoni & Schneider, 2010; Lindzen & Nigam, 1987). From a temporal perspective, the PC1 of this symmetrical mode exhibits a strong correlation with the Niño 3.4 index across six different reanalyzes. That is, the variation in the ENSO underpins the formation of HC EOF1. Moreover, an evident enhancement is observed in the variability of the ENSO after 1979, supporting the increased equatorially symmetrical variation in the HC. This result is further corroborated by the CMIP6 simulations. We see that the abilities of the models to reproduce the symmetrical mode are subject to whether they can well simulate the ENSO variability. Models that underestimate the ENSO variability cannot reproduce the connection between the ENSO and HC EOF1 and show large biases in simulating the dominant mode of the HC. The observed and modeled results consistently reveal that the regime shift of the HC variability is mainly due to the enhanced ENSO variability during the last 40 years.

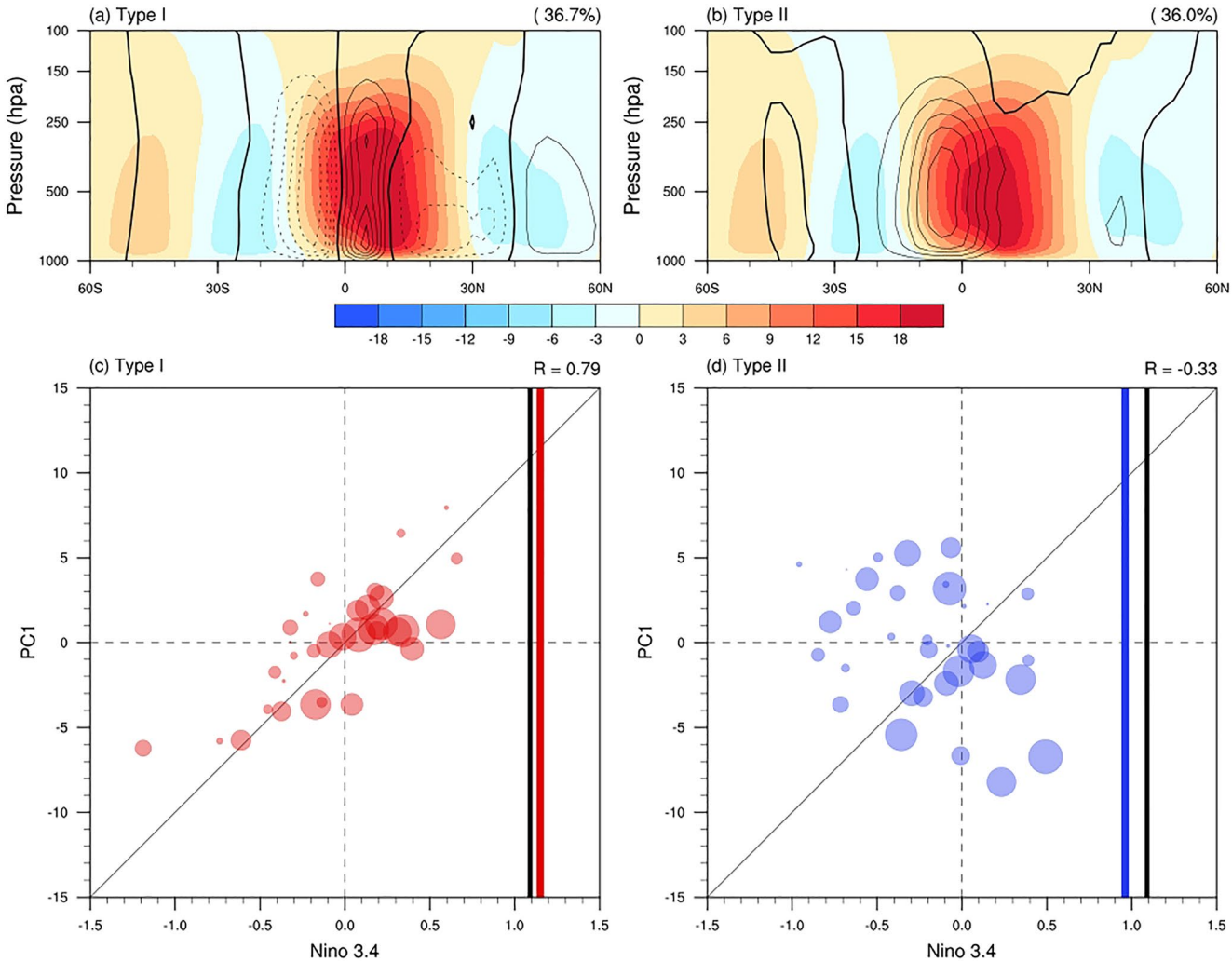

Figure 4. (a) Same as Figure 3a, but for the ensemble mean from the Type I models. (b) Same as (a), but from the Type II models. (c) Same as Figure 3b, but for the Type I models. The black and red lines indicate the standard deviation of the Niño 3.4 index calculated from HadISST and the ensemble mean of the Type I models, respectively. (d) Same as (c), but for the Type II models.

This study emphasizes the importance of the ENSO in modulating the HC variability. Notably, the SSTs in the tropical Indian Ocean are reported to be responsible for the first leading mode (i.e., the equatorially asymmetrical mode) of the seasonal HC (e.g., J. Li & Feng, 2015; Ma & Li, 2008); we see that there is little variation in the variability of tropical Indian Ocean SSTs. Conversely, the variability in the tropical central and eastern Pacific SSTs has become more active after 1979. It is of interest to further detect whether such a regime shift also occurs in other seasons. On the other hand, increased variability in the ENSO is projected under different greenhouse warming scenarios (Cai et al., 2022; Fredriksen et al., 2020; McGregor et al., 2022), and exploration of associated changes in HC variability would be worthwhile. Overall, our findings reveal that the increased ENSO variability contributes to the regime replacement in the HC variability, which may alter relevant convection and precipitation patterns, warranting additional research.

Data Availability Statement

Atmospheric reanalyzes including MERRA2, ERAI, ERA5, JRA55, CFSR, NCEP1, and NOAA-20CR used in the study are available at Gelaro et al. (2017), Dee et al. (2011), Hersbach et al. (2020), Kobayashi et al. (2015), Saha et al. (2010), Kalnay et al. (1996), and Compo et al. (2011). The SST data set from HadISST is available at Rayner et al. (2003). The AMIP and CMIP model's output analyzed in this study can be found in the Earth System Grid Federation (ESGF) repository (Cinquini et al., 2012).

Acknowledgments
This work was jointly supported by the National Key Research and Development Program of China (2023YFF0805100), the National Natural Science Foundation of China (42222501 and 41975079), the Fundamental Research Funds for the Central Universities (2233300001), the BNU-FGS Global Environmental Change Program (2023-GC-ZYTS-03), and the State Key Laboratory of Tropical Oceanography, South China Sea Institute of Oceanology, Chinese Academy of Sciences (LTO2310).

References

Alexander, M. A., Blade, I., Newman, M., Lanzante, J. R., Lau, N. C., & Scott, J. D. (2002). The atmospheric bridge: The influence of ENSO teleconnections on air-sea interaction over the global oceans. *Journal of Climate*, *15*(16), 2205–2231. https://doi.org/10.1175/1520-0442(2002)015<2205:TABTIO>2.0.CO;2

Bordoni, S., & Schneider, T. (2010). Regime transitions of steady and time-dependent Hadley circulations: Comparison of axisymmetric and eddy-permitting simulations. *Journal of the Atmospheric Sciences*, *67*(5), 1643–1654. https://doi.org/10.1175/2009JAS3294.1

Byrne, M. P., Pendergrass, A. G., Rapp, A. D., & Wodzicki, K. R. (2018). Response of the intertropical convergence zone to climate change: Location, width, and strength. *Current Climate Change Reports*, *4*, 355–370. https://doi.org/10.1007/s40641-018-0110-5

Cai, W., Ng, B., Wang, G., Santoso, A., Wu, L., & Yang, K. (2022). Increased ENSO sea surface temperature variability under four IPCC emission scenarios. *Nature Climate Change*, *12*(3), 228–231. https://doi.org/10.1038/s41558-022-01282-z

Capotondi, A., & Sardeshmukh, P. D. (2017). Is El Niño really changing? *Geophysical Research Letters*, *44*(16), 8548–8556. https://doi.org/10.1002/2017GL074515

Chang, E. (1995). The influence of Hadley circulation intensity changes on extratropical climate in an idealized model. *Journal of the Atmospheric Sciences*, *52*(11), 2006–2024. https://doi.org/10.1175/1520-0469(1995)052<2006:TIOHCI>2.0.CO;2

Chen, H., & Jin, F. (2020). Fundamental behavior of ENSO phase locking. *Journal of Climate*, *33*(5), 1953–1968. https://doi.org/10.1175/JCLI-D-19-0264.1

Cinquini, L., Crichton, D., Mattmann, C., Bell, G. M., Drach, B., Williams, D., et al. (2012). The Earth System Grid Federation: An open infrastructure for access to distributed geospatial data [Dataset]. Earth System Grid Federation (ESGF). Retrieved from https://esgf-node.llnl.gov/projects/esgf-llnl/

Clarke, A. J., & Van Gorder, S. (1994). On ENSO coastal currents and sea levels. *Journal of Physical Oceanography*, *24*(3), 661–680. https://doi.org/10.1175/1520-0485(1994)024<0661:OECCAS>2.0.CO;2

Compo, G. P., Whitaker, J. S., Sardeshmukh, P. D., Matsui, N., Allan, R. J., Yin, X., et al. (2011). The twentieth century reanalysis project. [Dataset]. National Center for Atmospheric Research Staff, *137*(654), 1–28. Retrieved from https://climatedataguide.ucar.edu/type/atmospheric-reanalysis/noaa-20cr

Dee, D. P., Uppala, S. M., Simmons, A. J., Berrisford, P., Poli, P., Kobayashi, S., et al. (2011). The ERA-interim reanalysis: Configuration and performance of the data assimilation system [Dataset]. European Centre for Medium-Range Weather Forecasts (ECMWF), *137*(656), 553–597. Retrieved from https://www.ecmwf.int/en/forecasts/dataset/ecmwf-reanalysis-interim

Deser, C., Phillips, A. S., Tomas, R. A., Okumura, Y. M., Alexander, M. A., Capotondi, A., et al. (2012). ENSO and Pacific decadal variability in the community climate system model version 4. *Journal of Climate*, *25*(8), 2622–2651. https://doi.org/10.1175/JCLI-D-11-00301.1

Fedorov, A. V., & Philander, S. G. (2001). A stability analysis of tropical ocean-atmosphere interactions: Bridging measurements and theory for El Niño. *Journal of Climate*, *14*, 3086–3101. https://doi.org/10.1175/1520-0442(2001)014<3086:ASAOTO>2.0.CO;2

Feng, J., Ji, X., Li, J., & He, E. (2023). Asymmetric impacts of El Niño development and decay stages on the Hadley circulation. *Geophysical Research Letters*, *50*(11), e2023GL103861. https://doi.org/10.1029/2023GL103861

Feng, J., & Li, J. (2013). Contrasting impacts of two types of ENSO on the boreal spring Hadley circulation. *Journal of Climate*, *26*(13), 4773–4789. https://doi.org/10.1175/JCLI-D-12-00298.1

Feng, J., Li, J., Jin, F., Liu, Z., & Zhao, S. (2019). Effect of El Niño on the response ratio of Hadley circulation to different SST meridional structures. *Climate Dynamics*, *53*(7–8), 3877–3891. https://doi.org/10.1007/s00382-019-04756-7

Feng, J., Li, J., & Xie, F. (2013). Long-term variation of the principal mode of boreal spring Hadley circulation linked to SST over the Indo-Pacific warm pool. *Journal of Climate*, *26*(2), 532–544. https://doi.org/10.1175/JCLI-D-12-00066.1

Fredriksen, H., Berner, J., Subramanian, A. C., & Capotondi, A. (2020). How does El Niño-Southern Oscillation change under global warming-a first look at CMIP6. *Geophysical Research Letters*, *47*(22), e2020GL090640. https://doi.org/10.1029/2020GL090640

Freund, R. J., & Wilson, W. J. (2003). *Statistical methods*. Academic Press.

Gelaro, R., McCarty, W., Suarez, M. J., Todling, R., Molod, A., Takacs, L., et al. (2017). The modern-ERA retrospective analysis for research and applications, version 2 (MERRA-2) [Dataset]. NASA GES DISC, *30*(14), 5419–5454. Retrieved from https://gmao.gsfc.nasa.gov/reanalysis/MERRA-2/data_access/

Gong, Y., Li, T., & Chen, L. (2020). Interdecadal modulation of ENSO amplitude by the Atlantic multi-decadal oscillation (AMO). *Climate Dynamics*, *55*(9–10), 2689–2702. https://doi.org/10.1007/s00382-020-05408-x

Grothe, P. R., Cobb, K. M., Liguori, G., Di Lorenzo, E., Capotondi, A., Lu, Y., et al. (2020). Enhanced El Niño-Southern Oscillation variability in recent decades. *Geophysical Research Letters*, *47*(7), e2019GL083906. https://doi.org/10.1029/2019GL083906

Guo, Y., Li, J., Feng, J., Xie, F., Sun, C., & Zheng, J. (2016). The multidecadal variability of the asymmetric mode of the boreal autumn Hadley circulation and its link to the Atlantic Multidecadal Oscillation. *Journal of Climate*, *29*(15), 5625–5641. https://doi.org/10.1175/JCLI-D-15-0025.1

Guo, Y., & Tan, Z. (2018). Relationship between El Niño-Southern Oscillation and the symmetry of the Hadley circulation: Role of the sea surface temperature annual cycle. *Journal of Climate*, *31*(13), 5319–5332. https://doi.org/10.1175/JCLI-D-17-0788.1

Gutzler, D. S., Kann, D. M., & Thornbrugh, C. (2002). Modulation of ENSO-based long-lead outlooks of southwestern US winter precipitation by the Pacific Decadal Oscillation. *Weather and Forecasting*, *17*(6), 1163–1172. https://doi.org/10.1175/1520-0434(2002)017<1163:MOEBLL>2.0.CO;2

Hari, V., Villarini, G., Karmakar, S., Wilcox, L. J., & Collins, M. (2020). Northward propagation of the intertropical convergence zone and strengthening of Indian summer monsoon rainfall. *Geophysical Research Letters*, *47*(23), e2020GL089823. https://doi.org/10.1029/2020GL089823

Held, I. M. (2001). The partitioning of the poleward energy transport between the tropical ocean and atmosphere. *Journal of the Atmospheric Sciences*, *58*(8), 943–948. https://doi.org/10.1175/1520-0469(2001)058<0943:TPOTPE>2.0.CO;2

Hersbach, H., Bell, B., Berrisford, P., Zhang, M., Horányi, A., Muñoz-Sabater, J., et al. (2020). The ERA5 global reanalysis [Dataset]. Copernicus Climate Change Service (C3S) Climate Data Store (CDS), *146*(730), 1999–2049. Retrieved from https://cds.climate.copernicus.eu/cdsapp#!/dataset/reanalysis-era5-pressure-levels-monthly-means?tab=overview

Higgins, R. W., Leetmaa, A., Xue, Y., & Barnston, A. (2000). Dominant factors influencing the seasonal predictability of US precipitation and surface air temperature. *Journal of Climate*, *13*(22), 3994–4017. https://doi.org/10.1175/1520-0442(2000)013<3994:DFITSP>2.0.CO;2

Hu, S., & Fedorov, A. (2018). Cross-equatorial winds control El Niño diversity and change. *Nature Climate Change*, *8*(9), 798–802. https://doi.org/10.1038/s41558-018-0248-0

Hu, S., Zhang, W., Jin, F., Hong, L., Jiang, F., & Stuecker, M. (2023). Seasonal dependence of the Pacific–North American teleconnection associated with ENSO and its interaction with the annual cycle. *Journal of Climate*, *36*(20), 7061–7072. https://doi.org/10.1175/jcli-d-23-0148.1

Hu, Z., Kumar, A., Ren, H., Wang, H., L'Heureux, M., & Jin, F. (2013). Weakened interannual variability in the tropical Pacific Ocean since 2000. *Journal of Climate*, *26*(8), 2601–2613. https://doi.org/10.1175/JCLI-D-12-00265.1

Kalnay, E., Kanamitsu, M., Kistler, R., Collins, W., Deaven, D., Gandin, L., et al. (1996). The NCEP/NCAR 40-year reanalysis project. *Bulletin of the American Meteorological Society*, *77*(3), 437–471. https://doi.org/10.1175/1520-0477(1996)077<0437:TNYRP>2.0.CO;2

Kang, S. M., Held, I. M., Frierson, D. M., & Zhao, M. (2008). The response of the ITCZ to extratropical thermal forcing: Idealized slab-ocean experiments with a GCM. *Journal of Climate*, *21*(14), 3521–3532. https://doi.org/10.1175/2007JCLI2146.1

Klein, S. A., Soden, B. J., & Lau, N. C. (1999). Remote sea surface temperature variations during ENSO: Evidence for a tropical atmospheric bridge. *Journal of Climate*, *12*(4), 917–932. https://doi.org/10.1175/1520-0442(1999)012<0917:RSSTVD>2.0.CO;2

Kobayashi, S., Ota, Y., Harada, Y., Ebita, A., Moriya, M., Onoda, H., et al. (2015). The JRA-55 reanalysis: General specifications and basic characteristics [Dataset]. Japan Meteorological Agency, *93*(1), 5–48. Retrieved from https://search.diasjp.net/en/dataset/JRA55

Krishnamurthy, V., & Goswami, B. N. (2000). Indian monsoon-ENSO relationship on interdecadal timescale. *Journal of Climate*, *13*(3), 579–595. https://doi.org/10.1175/1520-0442(2000)013<0579:IMEROI>2.0.CO;2

Kumar, A., & Hu, Z. (2014). How variable is the uncertainty in ENSO sea surface temperature prediction? *Journal of Climate*, *27*(7), 2779–2788. https://doi.org/10.1175/JCLI-D-13-00576.1

Kumar, K. K., Rajagopalan, B., & Cane, M. A. (1999). On the weakening relationship between the Indian monsoon and ENSO. *Science*, *284*(5423), 2156–2159. https://doi.org/10.1126/science.284.5423.2156

Lau, N. C. (1997). Interactions between global SST anomalies and the midlatitude atmospheric circulation. *Bulletin of the American Meteorological Society*, *78*(1), 21–33. https://doi.org/10.1175/1520-0477(1997)078<0021:IBGSAA>2.0.CO;2

Li, J., & Feng, J. (2015). Tropical large-scale atmosphere-ocean interaction in association with subtropical aridity trend. In F. Congbin (Ed.), *Aridity trend in northern China* (pp. 111–136). World Scientific Publishing Company Press.

Li, Y., Chen, Q., Liu, X., Li, J., Xing, N., Xie, F., et al. (2019). Long-term trend of the tropical Pacific trade winds under global warming and its causes. *Journal of Geophysical Research: Oceans*, *124*(4), 2626–2640. https://doi.org/10.1029/2018JC014603

Li, Y., Chen, Q., Xing, N., Cheng, Z., Qi, Y., Feng, F., & Li, M. (2021). Long-term trend of equatorial Atlantic zonal sea surface temperature gradient linked to the tropical Pacific cold tongue mode under global warming. *Journal of Geophysical Research: Oceans*, *126*(5), e2020JC017132. https://doi.org/10.1029/2020JC017132

Lindzen, R. S., & Nigam, S. (1987). On the role of sea-surface temperature-gradients in forcing low-level winds and convergence in the tropics. *Journal of the Atmospheric Sciences*, *44*(17), 2418–2436. https://doi.org/10.1175/1520-0469(1987)044<2418:OTROSS>2.0.CO;2

Lu, Y., Feng, J., Jia, F., & Hu, D. (2022). Interdecadal change in the relationship between the El Niño-Southern Oscillation and the north/south Pacific meridional mode. *Journal of Geophysical Research: Oceans*, *127*(7), e2021JC018284. https://doi.org/10.1029/2021JC018284

Ma, J., & Li, J. (2008). The principal modes of variability of the boreal winter Hadley cell. *Geophysical Research Letters*, *35*(1), L01808. https://doi.org/10.1029/2007GL031883

McGregor, S., Cassou, C., Kosaka, Y., & Phillips, A. S. (2022). Projected ENSO teleconnection changes in CMIP6. *Geophysical Research Letters*, *49*(11), e2021GL097511. https://doi.org/10.1029/2021GL097511

McGregor, S., Ramesh, N., Spence, P., England, M. H., McPhaden, M. J., & Santoso, A. (2013). Meridional movement of wind anomalies during ENSO events and their role in event termination. *Geophysical Research Letters*, *40*(4), 749–754. https://doi.org/10.1002/grl.50136

McPhaden, M. J., Lee, T., & McClurg, D. (2011). El Niño and its relationship to changing background conditions in the tropical Pacific Ocean. *Geophysical Research Letters*, *38*(15), L15709. https://doi.org/10.1029/2011GL048275

Nguyen, H., Evans, A., Lucas, C., Smith, I., & Timbal, B. (2013). The Hadley circulation in reanalyses: Climatology, variability, and change. *Journal of Climate*, *26*(10), 3357–3376. https://doi.org/10.1175/JCLI-D-12-00224.1

Numaguti, A. (1994). Dynamics and energy balance of the Hadley circulation and the tropical precipitaton zones, Part II: Sensitivity to meridional SST distribution. *Journal of the Atmospheric Sciences*, *52*(8), 1128–1141. https://doi.org/10.1175/1520-0469(1995)052<1128:daebot>2.0.co;2

Oort, A. H., & Yienger, J. J. (1996). Observed interannual variability in the Hadley circulation and its connection to ENSO. *Journal of Climate*, *9*(11), 2751–2767. https://doi.org/10.1175/1520-0442(1996)009<2751:OIVITH>2.0.CO;2

Peng, Q., Xie, S., Wang, D., Kamae, Y., Zhang, H., Hu, S., et al. (2020). Eastern Pacific wind effect on the evolution of El Niño: Implications for ENSO diversity. *Journal of Climate*, *33*(8), 3197–3212. https://doi.org/10.1175/JCLI-D-19-0435.1

Peng, Q., Xie, S., Wang, D., Zheng, X., & Zhang, H. (2019). Coupled ocean-atmosphere dynamics of the 2017 extreme coastal El Niño. *Nature Communications*, *10*(1), 298. https://doi.org/10.1038/s41467-018-08258-8

Rayner, N. A., Parker, D. E., Horton, E. B., Folland, C. K., Alexander, L. V., Rowell, D. P., et al. (2003). Global analyses of sea surface temperature, sea ice, and night marine air temperature since the late nineteenth century [Dataset]. The UK Met Office, *108*(D14). Retrieved from http://www.metoffice.gov.uk/hadobs/hadisst/data/download.html

Saha, S., Moorthi, S., Pan, H., Wu, X., Wang, J., Nadiga, S., et al. (2010). The NECP climate forecast system reanalysis [Dataset]. National Center for Atmospheric Research Staff. Retrieved from https://climatedataguide.ucar.edu/climate-data/climate-forecast-system-reanalysis-cfsr

Schneider, E., & Lindzen, R. S. (1977). Axially symmetric steady state models of the basic state of instability and climate studies. Part I: Linearized calculations. *Journal of the Atmospheric Sciences*, *34*, 253–279.

Schneider, T., Bischoff, T., & Haug, G. H. (2014). Migrations and dynamics of the intertropical convergence zone. *Nature*, *513*(7516), 45–53. https://doi.org/10.1038/nature13636

Sun, Y., Li, L. Z. X., Ramstein, G., Zhou, T., Tan, N., Kageyama, M., & Wang, S. (2019). Regional meridional cells governing the interannual variability of the Hadley circulation in boreal winter. *Climate Dynamics*, *52*(1–2), 831–853. https://doi.org/10.1007/s00382-018-4263-7

Sun, Y., & Zhou, T. (2014). How does El Niño affect the interannual variability of the boreal summer Hadley circulation? *Journal of Climate*, *27*(7), 2622–2642. https://doi.org/10.1175/JCLI-D-13-00277.1

Terray, P., & Dominiak, S. (2005). Indian Ocean sea surface temperature and El Niño-Southern Oscillation: A new perspective. *Journal of Climate*, *18*(9), 1351–1368. https://doi.org/10.1175/JCLI3338.1

Trenberth, K. E., Branstator, G. W., Karoly, D., Kumar, A., Lau, N. C., & Ropelewski, C. (1998). Progress during TOGA in understanding and modeling global teleconnections associated with tropical sea surface temperatures. *Journal of Geophysical Research*, *103*(C7), 14291–14324. https://doi.org/10.1029/97JC01444

Wallace, J. M., Rasmusson, E. M., Mitchell, T. P., Kousky, V. E., Sarachik, E. S., & von Storch, H. (1998). The structure and evolution of ENSO-related climate variability in the tropical Pacific: Lessons from TOGA. *Journal of Geophysical Research*, *103*(C7), 14241–14259. https://doi.org/10.1029/97JC02905

Wang, B., & An, S. I. (2001). Why the properties of El Niño changed during the late 1970s. *Geophysical Research Letters*, *28*(19), 3709–3712. https://doi.org/10.1029/2001GL012862

Zhang, W., Jiang, F., Stuecker, M. F., Jin, F., & Timmermann, A. (2021). Spurious north tropical Atlantic precursors to El Niño. *Nature Communications*, *12*(1), 3096. https://doi.org/10.1038/s41467-021-23411-6

Zhang, W., Jin, F., Zhao, J., & Li, J. (2013). On the bias in simulated ENSO SSTA meridional widths of CMIP3 models. *Journal of Climate*, *26*(10), 3173–3186. https://doi.org/10.1175/JCLI-D-12-00347.1

Zhang, W., Wang, Z., Stuecker, M. F., Turner, A., Jin, F.-F., & Geng, X. (2019). Impact of ENSO longitudinal position on teleconnections to the NAO. *Climate Dynamics*, *52*(1–2), 257–274. https://doi.org/10.1007/s00382-018-4135-1